HEAT TRANSFER ON BLUNTED BODIES IN A HIGH-SPEED DUSTED FLOW

E.B. Vasilevskiy, L.V. Yakovleva
Central Aerohydrodynamic Institute

high-speed dusty flow

Abstract

A comprehensive experimental investigation of heat transfer in a two-phase flow past spherical and cylindrical models was carried out in a short duration wind tunnel at Mach number M_∞=6, Reynolds number based on the free-stream flow parameters and the model radius $Re_{\infty R}$ = (4 ÷ 500)∗10^3, for different gases (N_2, CO_2, air), and free-stream particle mass concentration c ranging from 1% to 25%. Particles of SiO_2, Cr_2O_3, Fe_2O_3, Si_3N_4, and Fe, with a diameter ranging from 0.12 μm to 2.4 μm were used. Use was also made of hollow SiO_2 spheres with an external diameter of 160 μm and wall thickness of ~ 5 μm.

1 Introduction

Interaction of a high-speed dusty flow with a blunted body arises from high-speed motion of bodies in dusty atmosphere, dusty flow over structural elements of solid-propellant engines nozzles, cutting of materials by a supersonic dusty jet, and in many other cases.

When a body is in gas flow with condensed particles, a variety of physical effects can occur: increase in the particle concentration near the front body surface by orders of magnitude [1]; increase in heat transfer between a dusty gas flow and a body in flow by many times [2-4]; powerful optical flow radiation near the body surface; significant electrization of the body surface and particles (to several kV and more), [5,6]; sticking of particles to the body surface, penetration of particles into the external body layer or intense erosion of the body surface [7, 8].

Dusty gas flow over bodies is of much more complicated nature as compared with a pure gas flow over bodies. Due to inertia of dust particles, their trajectories can differ essentially from gas stream lines.

Depending on particle inertia and state, three qualitatively different flow patterns may take place: a) large solid particles whose inertia is fairly high are almost not braked in the shock layer, reach the body surface, and then rebound forming a layer of reflected particles; b) for particles with moderate inertia (or molten particles) the typical is the situation in which a thin layer (or a film) is formed by deposited particles on the frontal surface of the body; c) for very small size or low density of the particles (small inertia), the velocity slip between the phases is so small that the almost all particles do not reach the body surface. In the latter regime the particle trajectories envelop the frontal surface of the body (the regime of absence of particle inertial deposition).

Hence the presence of even small amount of condensed particles in the free stream may drastically change the flow and heat transfer near the frontal surface of a blunt body immersed in a supersonic flow.

In cases a) and b), the main heat transfer intensification mechanisms are: the conversion of the particle kinetic energy into the thermal energy of the body, turbulization of the boundary layer by the wakes behind inertial particles, and additional turbulization due to the roughness of the body surface caused by impinging particles. The heat transfer in flows with inertial particles was investigated in [11-15]. In most of these studies the particle size was greater than 20 μm. For case c), a theoretical analysis of the two-phase boundary layer on a blunt body in hypersonic flow indicates that fine non-depositing particles (for instance, for a 1 m body moving at a supersonic

velocity at an altitude of 10 km, the particles less than several microns in size) may result in a noticeable increase in the heat flux due to particle accumulation near the frontal surface of the body [14]. The first results of experimental study of the heat transfer for flow regime c) [2-4] have confirmed the theoretical results [14, 15].

In this paper, we present the experimental results for the heat transfer on the frontal surface of a sphere and a cylinder in a supersonic dusty-gas flow for a wide range of variation of the particle inertia parameter, including the regime of absence of particle inertial deposition.

2. Experimental facilities

2.1 Wind Tunnel

The high pressure channel of the wind tunnel with the inner diameter 70 mm and length 6 or 12 m was equipped by an external ohmic heater which provides gas heating up to T_0 = 800 K, Fig. 1. The test section diameter is 0.5 m. Duration of the steady-state flow was τ = 23 ms or 46 ms.

For introducing the particles into the flow, we used the “fluidized bed” method, Fig. 2. As a rule the mixer 7 was installed in one inlet used to introduce the dusty gas into the wind tunnel section located near diaphragms 2 of the UT-1 tunnel. The inner channel of the mixer is shaped as a vertical cone with the half apex angle of

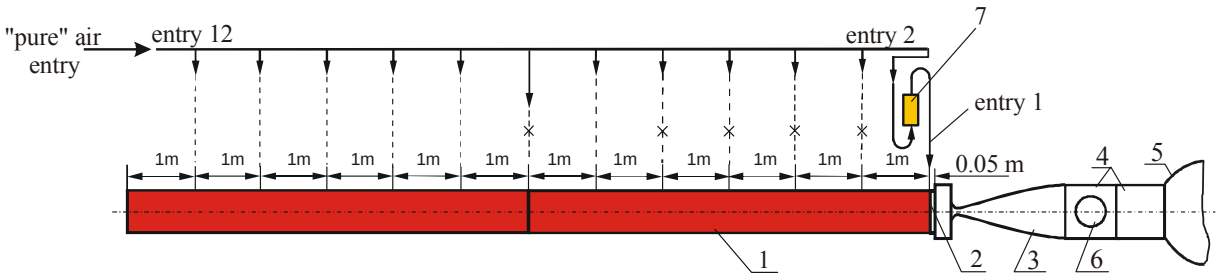

Fig. 1. Wind tunnel UT-1. 1 – duct, 2 – diaphragm, 3 – nozzle, 4 – test section, 5 – exhaust chamber, 6 – optical window, 7 – mixing device.

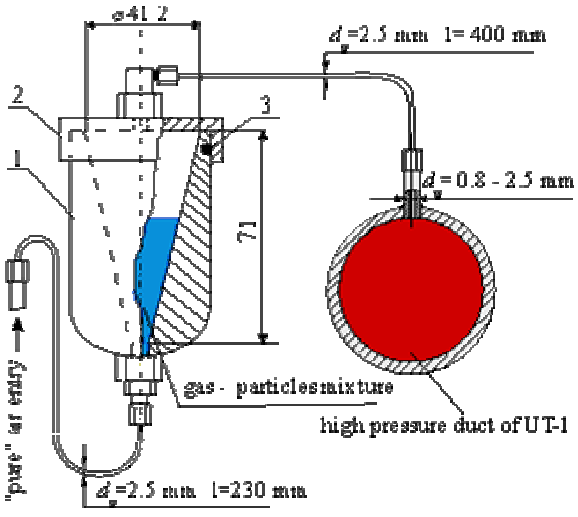

Fig. 2. Mixing device.

15° and 71 mm high**.** The cone outlet diameter is 41 mm. At the outlet section of the cone, as a rule, was mounted a perforated membrane with hole diameter of 2 mm and the step between holes of 5 mm. The mixer volume was 36 cm^3. At the beginning of an experiment, volume of the dust was from 1 to 10 cm^3.

The estimates show that even at maximum duration of the steady-state flow, the air flowing through the nozzle occupies only the front part of the high-pressure channel (about 3 m in length) situated near the diaphragm and the nozzle. Therefore it is expedient to fill by the dust only the front part of the channel. At the end of each test (at $\tau \gtrsim$46 ms)) partial cleaning of the front channel from the particles by "clean" air expiring from rear part of the channel. If the tests conditions do not change,

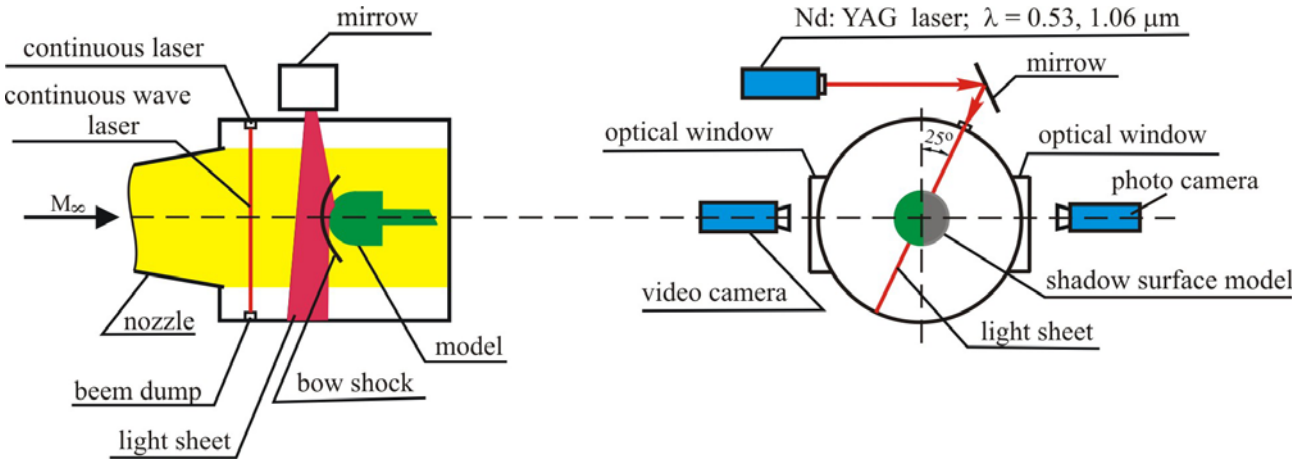

Fig. 3. Optic scheme.

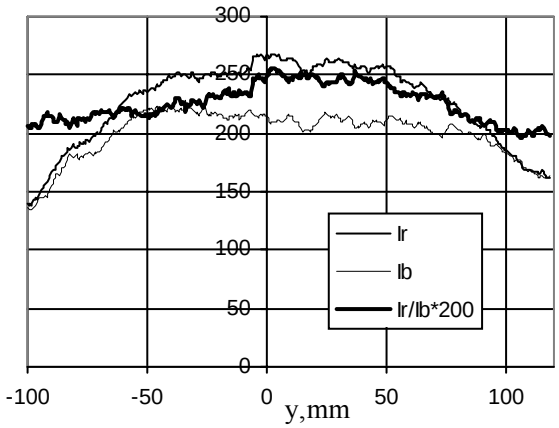

Fig. 4. Distribution of light intensity in infrared (Ir), green (Ib) intervals and ratio Ir/(Ib*200) in cross section of free flow, Fe_2O_3, R_n= 150 мм.

such test technology provides good repeatability of particles concentration and heat exchange beginning from the third test.

To examine the particle parameters in the nozzle flow, a quasi-one-dimensional dusty-gas flow in the internal duct of the wind tunnel UT-1 was simulated numerically [4,17]. Calculations have shown that for the particles used their thermal and speed sliding relative the carrying phase did not exceed 2 %.

For investigation of free dusted gas flow and particles flow near the body surface, it was used both a shadow method and a method based on registration of scattered light. Fig. 3 presents a scheme in which the light sheet («laser knife») was used.

The radiation intensity distribution in cross section of the free flow (ahead the bow shock wave) is presented on Fig. 4.

At small volumetric concentration of particles, intensity of the scattered light is proportional to the particle concentration, and the ratio of intensities of two wavelengths Ir/Ib characterizes the mean particle size. This data show that the concentration distribution is approximately uniform in the jet core which is 150 mm in diameter. The intensity ratio of thediffused light "Ir/Ib" in the jet core is approximately uniform, too. It testifies that the average size of particles in the cross section of the jet core is also approximately constant.

The presented data are obtained at short exposition which is approximately 10^5 times smaller than the characteristic sensitivity time τ_{cal} of the calorimetric gauges used. Estimations show that concentration alterations during the period of $\tau \approx \tau_{cal}$ does not exceed some percents.

The particles concentration was registered depend during a run by the red-color photodiode laser (wave length of 0.65 μm) with the power of 2 mW. The laser was located near the upper surface of the test section. With the help of a mirror, the light beam crossed the gas flow from top to bottom. Near the bottom surface of the test section, a "light trap" was mounted, which reduces intensity of the light reflected from the surface of the test section. To transform the

PEM signal into the particle weight flow, we assumed the following:

- particles weight flow is directly proportional to the signal recorded,
- particles concentration is constant across the jet section,
- total powder amount in the mixer before the test is entrained by the gas flow to the end of registering the test parameters.

With account of these assumptions we can write:

$$G_p = k \int_0^{\tau} J d\tau$$

where, G_p is the powder weight in the mixer before the test, J is the current value of the signal, and τ is the current time. This formula was sued for determining the value of the coefficient k for a given test. The current particles concentration was determined from the formula:

$$c_\tau = (k \bullet J)/(\pi \rho_\infty u_\infty R_w^2)$$

The example of registration with the help of the given system is shown on Fig. 5.

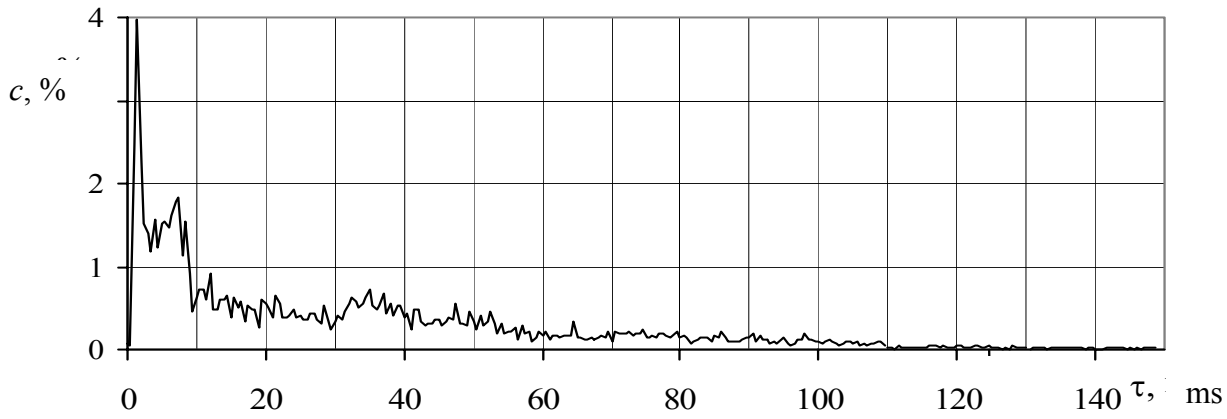

Fig. 5. The weight concentration of particles in the jet core n during run.

2.2. Particles

Different compositions of the particles were used in the tests. The main particle parameters are summarized in Table 1.

Table 1

Particles used in the tests.

	d_n	d_m	e	ρ_p	c_p
---	μm	μm		kg/m^3	J/(kg)
SiO_2	0.15	0.19	0.047	2264	1059
Si_3N_4	0.12	0.16	0.061	3440	≈1000
Fe_2O_3	0.27	0.37	0.244	5250	881
Cr_2O_3	0.75	1.36	1.61_	5210	802
Fe (2nd lot)	0.95	1.2_	1.8__	7874	574
Fe (1st lot)	2.40	4.6_	20.8_	7874	574
*SiO2	161	187	1220 __	324	1059

*SiO_2 - hollow sphere.

Here, $d_n = [(\Sigma d_i^3 * n_i)/(\Sigma n_i)]^{1/3}$ is the mean particles diameter,

$d_m = \Sigma d_i \cdot p_i$ is the mean mass particles diameter,

$e = (d_m^2 u_\infty \rho_p \psi)/27 \mu_s R_w)$ is the particle inertia

d and ρ_p - diameter and density of a particle, u-velocity, indexes ∞ and s - in free flow and behind a shock wave, ψ is the correction factor, which takes the Knudsen effects Kn in the particle Stocks drag into account [2], $\Psi = 1 + Kn(2{,}492 + 0{,}84 exp(-1{,}74/Kn))$,

$Kn = \lambda_s / d$, $\lambda_s = 1.255 \mu_s / [\rho (R_g T_s)^{0.5}]$, μ_s and λ_s - viscosity and free path of gas molecular behind a bow shock.

Note that the SiO_2 particles were both solid spheres with a mean diameter d = 0.15 μm and hollow spheres with a mean diameter d = 160 μm and wall thickness ~5 μm.

In table 1 the particle inertia e was calculated for the air flow at Mach number M=6, the stagnation temperature T_0=600 K, full

pressure P_0=20 bar, the radius of the sphere nose R_w=12 mm. Particles have the no-deposition regime at the particle inertia about $e \leq 0.05$

The particle characteristics were measured using a PHILIPS SEM-515 scanning electron microscope. The particle weight distribution $S_j=\Sigma_j(d_i p_i / d_m)$ as a function of the nondimensional particle diameter d/d_m is shown in Fig. 6.

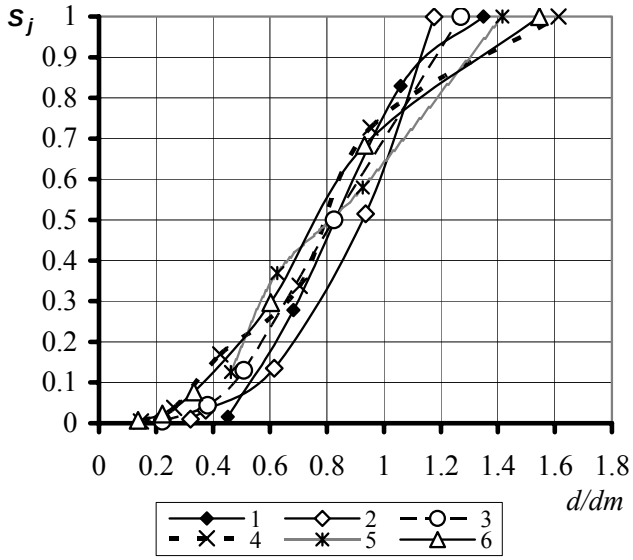

Fig 6. The weight distribution of particles vs. nondimensional particle diameter d/d_m. 1-*SiO_2, 2- SiO_2, 3- Si_3N_4, 4- Cr_2O_3,5- Fe_2O_3, 6- Fe (1st lot)

All particles were approximately spherical, except for the Fe_2O_3 and Cr_2O_3 particles.

In order to eliminate the coagulation, before the tests the powder was dried in a thermostat at 450 °K, divided into portions, wrapped in a metal foil and stored in an exsiccator with $CaCl_2$ drier, which ensured a residual pressure of water vapor below 0.34 mm Hg.

2.3 Models

For carrying out of researches 4 various models were used: the model "A" is spheres installed on the same suspension arm; the model "B" is the cylinder with smooth spherical blunted nose; the model "C" is cylinder with spherical blunted nose, having the small ledge on the frontal surface (the device for tangential injection), [16]; the model "D" is plate with the cylindrical forward edge.

The model “A" has consisted of four aluminum spheres with radii R_w=3, 6, 12, and 24 mm installed on the same suspension arm. The distance from the critical point of each sphere up to the nozzle exit section made 41 mm.

The frontal surfaces of all the spheres were located in one plane perpendicular to the jet axis at a distance of 150 mm from the nozzle exit. The azimuthal angle between the spheres was 90°.

At the stagnation point of each sphere, a calorimetric heat flux gage was installed. A brass disk of 2 mm in diameter with thickness of almost 0.3 mm served as its sensitive element. The disk was pasted into a paper sleeve with the diameter of 2.5 mm. The sleeve was pasted, in turn, into the relevant model orifice. Then each gage was polished flush with the spherical model surface. A 0.1 mm-junction of chrome and copal wires was welded on the internal surface of the brass disk. Before welding, the thermocouple junction was expanded to the thickness of 0.03 mm and cut to the width of 0.3 mm. This design of the calorimetric gage ensured an essentially linear dependence of the heat flux on the electric signal growth rate within 40 ms.

For each calorimetric gage, the gage sensitivity coefficient was determined using a special calibration facility of TsAGI.

The model "B" was the cylinder with smooth spherical blunted nose. This aluminium model with radius R_w = 25 mm was equipped with calorimeters, Fig. 7.

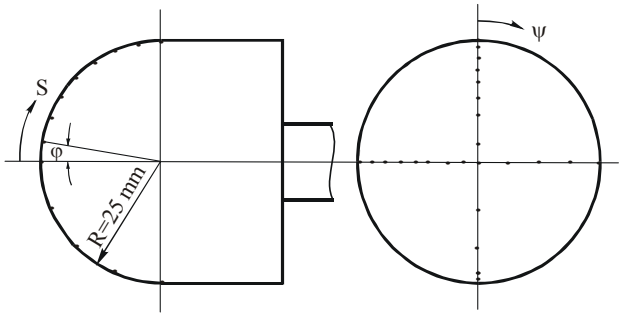

Fig. 7. Calorimetrical model “B”. The cylinder with spherical nose. Dots − calorimeters.

The angle step between calorimeters along the sphere generatrix is 15° (including the calorimeter in the stagnation point).

The model “C” represents itself a spherically blunted cylinder (Fig. 8). The model had the device "cap", located near to a critical point. This device created a small ledge. The size of the ledge on an axis of model (at height of a slot $h_k = 0$) was 1.5 mm. The recess on the edge of "cap" (at central angle $\varphi = 15°$) was $h_w = 0.6$ mm.

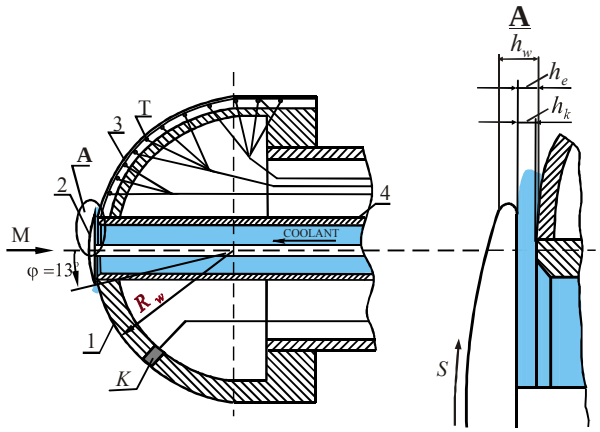

Fig. 8. Model “C”. The cylinder with spherical nose. Dots − calorimeters.

The model "D" represented itself a plate with a cylindrical forward edge. The length of model along a flow was 100 mm. The length of generatrix of the cylinder was 150 mm. The radius of the cylindrical model was $R_w = 15$ mm.

The heat flux was measured by the thin wall technique. A stainless steel foil band 21 mm (по потоку) in width and 0.2 mm in thickness was welded to the cylindrical model surface. On the inside, 0.1-diameter wires from kopel alloy were welded to the foil. Near the welding point, the wires were expanded up to the thickness of 0.03 -0.04 mm. The dimensions of the thermocouple contact zone were 0.2 mm x 0.2 mm. The model nose has been prepared by 72 thermocouples. The step between welding points on a frontal surface of the cylinder has was 0.7 mm (2.7 °).

2.4 Test conditions

The basic test conditions for model **a)** are given in table 2.

Table 2

Basic test conditions

Parameter	Value
*Working gas	Air
Mach number (air) M_∞	6
*Total pressure P_o	17.5 bar
Stagnation temperature T_o	570 °K
Exit diameter of a nozzle	300 mm
*Model	4 spheres
*Substance of particles	Solid SiO_2
*Mass concentration of particles in the flow, c	3 %

When the test conditions were changed, as a rule, only one of the parameters denoted by * in Table 2 was varied. The variants of the test conditions are given in table 3.

Table 3

Variants of test conditions

Model	Gas	Particles	P_o, bar	c,%
"A" "B" “C”	Air	SiO_2	2.1	≈1
				≈25
			7.8	≈1
			17.5	≈1
				≈3
				≈6
			33.0	≈1
		*SiO_2	17.5	≈3
		Fe_2O_3		
		Cr_2O_3		
		Si_3N_3		
		Fe_4		
	N_2	SiO_2	17.5	≈3
	CO_2			
"D"	air	Fe_2O_3	17.5	≈2

*SiO_2 - hollow sphere.

3. Experimental results

When the particles are present in the flow, the temperature growth rate registered by the

calorimetric gages ΔT is considerably higher than in the pure gas flow. Fig. 9 exemplifies the measured temperature at the stagnation point vs. time for the sphere with radius R_w=6 mm in flows with and without particles.

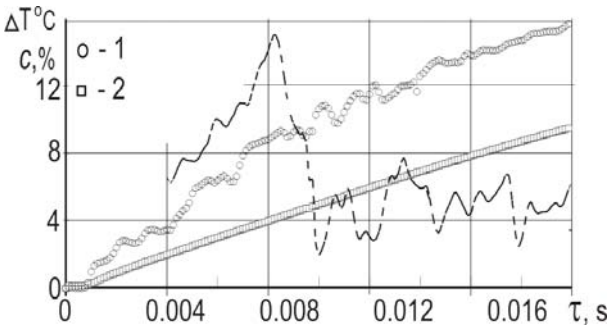

Fig. 9. Particle concentration and the temperature of a calorimeter vs. time. Model "A", Fe_2O_3, R_w = 24 mm, T_0=570 K, P_0=33 bar.

Clearly, being approximately equal to that in pure gas flow at the beginning of the tests, the calorimeter temperature in the dusty gas flow at the end of the test is in 1.5 times higher than in the pure gas. Besides, the temperature growth curve is smooth in the pure gas flow and irregular in the flow with the particles. This is caused by both variations in the free-stream particle concentration during the test and electrical disturbances due to electrostatic phenomena occurring near the model surface in the dusty gas flow. Assuming that (i) the electrical disturbances are random in nature and (ii) the mean level of resulting additional voltage in the measuring channels of the calorimeters is zero, it is possible to substantially reduce the effect of electrical disturbances on the recorded heat flux q at a high scanning rate (8 kHz). The ratio of the heat flux q/q_0 as a function of the current particle concentration ahead of the bow shock wave during the test is presented in Fig. 10.

It is clear that the heat flux ratio $q/q0$ increases with concentration c approximately by a linear law. The further analysis of the measured heat flux and particle concentration was carried out for the heat flux and concentration values averaged over a period from 4 ms to 20 ms.

This averaging significantly reduces the effect of electrical disturbances in the dusty gas flow on the thermocouple readings. The initial time interval τ<4 ms, when various unsteady processes (associated with the attainment of a regular regime) could be significant, was excluded from the consideration. To obtain more reliable results, the tests were repeated 3-6 times for each regime.

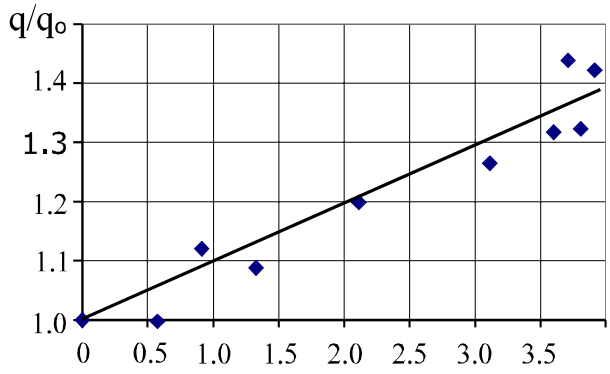

Fig. 10. The heat flux q/q_0 as a function of the current particle concentration c. Model "A", SiO_{32}, R_w = 24 mm, R_w = 6 mm, T_0=570 K, P_0=17.5 bar.

Below, we represent only the data averaged in accordance with the procedure described above.

The tests showed that the presence of even very fine solid particles of SiO_2 with dm= 0.19 μm in the air flow results in an appreciable increase in the heat fluxes. The relative heat flux increases also with increase in the full pressure (Fig. 11).Fig. 11. The relative heat flux vs. particle concentration.

Model "A". R_w = 6 mm, T_0=570 K.

The increase in particle inertia (decrease in

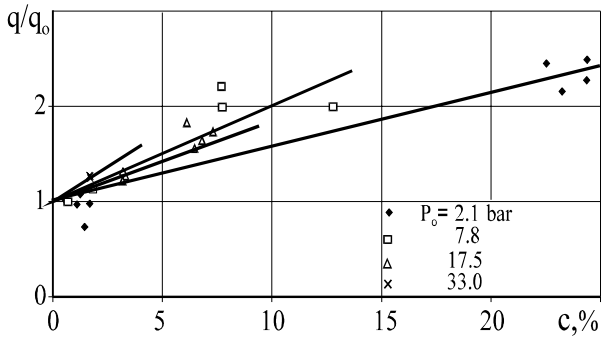

e results in a considerable increase in the heat flux q/q_o even at small mass concentrations (Fig. 12). The dependence of the heat flux on the sphere radius turns out to be non-monotonous.

It is caused by complex influence of nose radius R_w on heat exchange in the dusty gas flow. With increase in radius of streamline body R_w the convective heat flux in a pure gas flow

decreases q ~ $1/R_w^{0.5}$. At the same time, with increase R_w thickness of a shock layer proportionally increases. Thereof speed of impact of particles about the body surface decreases exponentially. Due to the thermal flux caused by particles decreases approximately exponentially too.

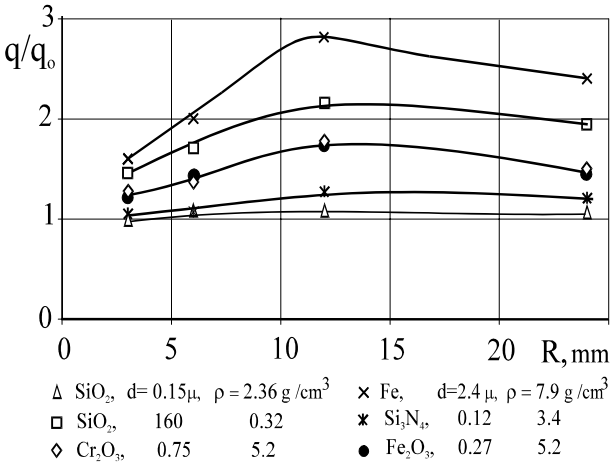

Fig. 12. The heat flux q/q_0 vs. sphere radius R_w.
Model "A", Air, P_0 = 17.5 bar, T_0=570 K, c = 1%.

The heat flux distribution on the front spherical surface of the model "B" is shown on Fig. 13-15 for various conditions: in the pure flow and at presence of solid particles Fe (2nd lot).

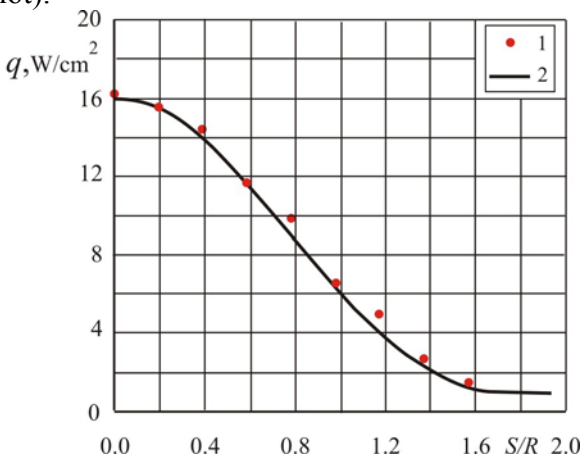

Fig. 13. Distribution of heat flux on the cylinder with the spherical nose in clean gas flow.
Model "B". Fe (2nd lot), T_0 = 600 K, P_0 = 24 bar.
dots –experiments ; 2 – calculation [3]

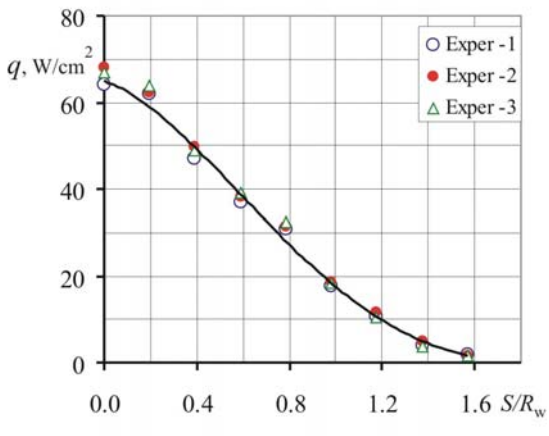

Fig. 14 Distribution of heat flux on the cylinder with the spherical nose in dusted gas flow.
Model "B". Fe (1st lot), T_0 = 600 K, P_0 = 24 bar,
c_m = 1,5 %

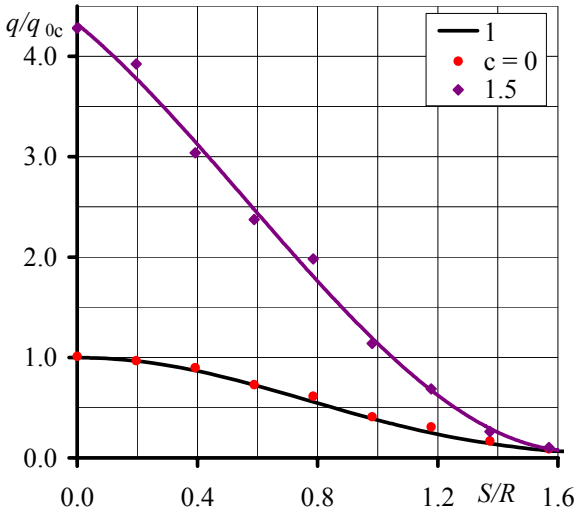

Fig. 15. The ratio of heat flux in the given point of the surface at the dusted flow to the heat flux in this point at the clean gas flow.
Model "B". Fe (2nd lot), T_0 = 600 K, P_0 = 24 bar.
1 – calculation [10]. Dots – experiments.

Analogy results were obtained for model "C" and "D" in flow with small inertia particles.

Fig. 16 illustrates the ratio of the heat flux ratio obtained in the experiments with particles q to the heat flux at the same surface point but without particles (in pure flow) q_0 on the model "C" surface. It is seen that on the whole front surface of the sphere bluntness as far as the central angle of about 80°(S/R_w = 1.4).

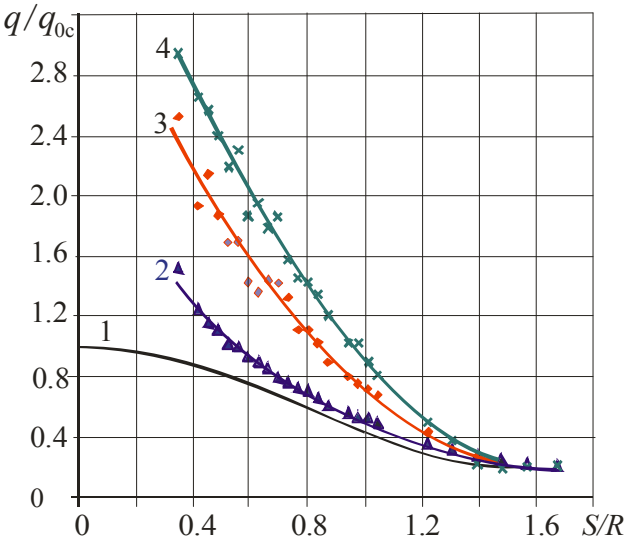

Fig. 16. The ratio of heat flux in the given point of the surface to the calculated heat flux at critical point of body. Model "C". Fe_2O_3, 1-calculanted for smooth surface at laminar boundary layer; 2 – n_m = 0; 3 – n_m = 1.4 %; 4 – n_m = 2.6 %.

On Fig. 17 it is shown the ratio of heat flux in the given point of the surface to the calculated heat flux at critical point of body for smooth surface at laminar boundary layer (curve 1). Experimental results at pure gas at near critical point exceed calculated value. This effect is due to the fact that the dripping boundary layer from "cap" (see Fig. 8) is appended to the sphere surface. The presence of particles Fe_2O_3 at small weight concentration sufficiently increases the heat flux to the body surface.

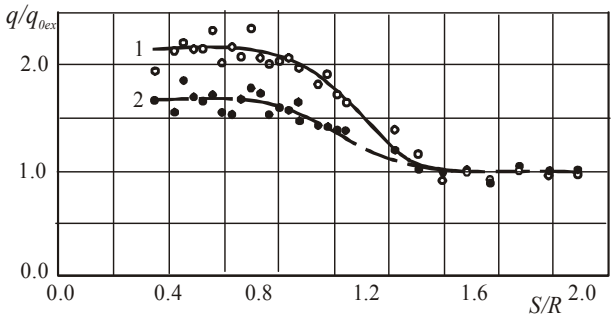

Fig. 17. The ratio of heat flux in the given point of the surface at the dusted flow to the heat flux in this point at the clean gas flow. Model "C". Fe_2O_3, 1 – c_m = 2.6 %; 2 – c_m = 1.4 %, R_w = 37.5 mm.

At S/R_w= 0.7 increase in the heat flux is constant to be q/q_0 =1.7 at concentration n_m = 1.4 % (curve 2) and q/q_0 = 2.2 at concentration n_m = 2.6 % (curve 1).

Such noticeable effect of particles with low inertia (small particle size with respect to the body size) on heat exchange is caused by the fact that the particles lose a significant part of their kinetic energy in the boundary layer of gas and increase the flow enthalpy near the body surface in flow. Besides, the particles transfer the attached high-temperature gas flow mass to the boundary layer part adjacent to the surface, as well as cause its turbulization [2,17.

The increase in the heat fluxes takes place only on the frontal surface of the model. As an example, in Fig. 18 the distribution of the heat fluxes over the cylinder (model "D") is presented. As is clear, the influence of particles on the heat flux is significant up to approximately 50°.

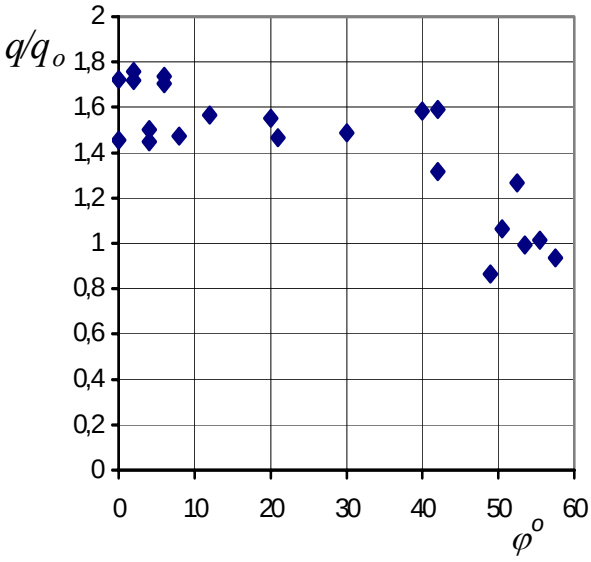

Fig. 18 The ratio of heat flux in the given point of the surface at the dusted flow to the heat flux in this point at the clean gas flow. Model "D", Fe_2O_3,

Conclusions

The experiments in a short-duration wind tunnel demonstrated that the presence of small solid particles (microns and fractions of micron in size) in the supersonic (M=6) gas flow results in a considerable (up to 3 times) increase in the heat fluxes to the frontal surface of a blunt body immersed in the flow even for small free-stream particle mass concentration (of the order of several percents). The effect of heating augmentation increases with increase in particle inertia. The heat flux almost linearly increases with particle concentration. The increase in the

heat fluxes occurs only on the frontal surface of a blunt body.

Acknowledgements

This work is supported by the Russian Foundation for Basic Research RFBR (grants No. 10-01-00745-a, 10-01-91332-NNIO_a).

8. References

[1] Vasilevskii, E. et al. Diagnostics of supersonic dusted flow near a blunt body. *In XII Intern. Conf. on the Methods of Aerophysical Research*; 28 June-3 July, 2004, Novosibirsk, Russia, p. 299-304.

[2] Vasilevskii, E.B. and Osiptsov, A.N. Experimental and numerical study of heat transfer on a blunt body in dusty hypersonic flow. *AIAA Paper* N 99-3563, 1999, p. 1-11.

[3] Vasilevskii, E. at al. Heat exchange on the front surface of a blunt body in a high-speed flow containing low-inertia particles. *Journal of Engineering Physics and Thermophysics*, 74, 2001, No. 6, p. 34-42.

[4] Vasilevsky, E. et al. Heat Transfer in a Heterogeneous Supersonic Flow, Proc. *In 12th Intern. Heat Transfer Conf.,* Grenoble, France, August 18-23, 2002, vol. 3, p. 177-181.

[5] Vasilevskii, E. at al. Body electrization in a supersonic two-phase flow. *In Proc. of Second Inter. Conf. "Materials and Coating for Extreme Performances: Investigations, Applications, Ecologically Safe Technologies for Their Production and Utilization.* 16-20 Sept. 2002, Katseveli-town, Crimea, Ukraine, p. 23-24.

[6] Joseph C. Kolecki, Barry Hillard, Mark Sielbert. *Overview of Mars System-Environment Interactions* AIAA Paper 96-2333, 1996.

[7] D. Mikhatulin, Y. Polezhaev, L. Reviznikov. Thermo-Erosion Destruction of Materials in Supersonic Heterogeneous Flows. *Proceeding of European Conference for Aero-Space Sciences, July 4–7th 2005, Moscow*, CD, No 4.04.06, p. 1-9.

[8] E.B. Vasilevskii, T.V. Ershova, D.S. Mikhatulin, L.V. Yakovleva. The physical effects arising at interaction of a high-speed dusty flow with a blunted body. *Proceeding of 2ND European Conference for AeroSpace Sciences (EUCASS)*, July 1-6th, 2007, Brussels, Belgium.

[9]`Mikhatulin D.S., Polezhaev Yu.V., Repin I.V., Heterogeneous Streams: Gasdynamics, Heat Transfer, Erosion, *Preprint IVTAN 2-402, RAS Institute for high temperature*, Moscow, 1997.

[10]`Fleener W.A. and Watson R.H., Convective heating in dust laden hypersonic flows. *AIAA Paper 73-761*, 1973.

[11]Dunbar L.E., Courtney J.F., and McMillen. L.D., Heating augmentation in erosive hypersonic environments. *AIAA J.*, V.13, No. 7, pp. 908-912, 1975.

[12]Shih W.C.L, Ballistic range measurements of aerodynamic heating in erosion environments. *AIAA Paper 76-319*, 1976.

[13]Yu H.R , Li Z.F, and Lin J.M. Shock tube measurements of stagnation point heat transfer rates in dusty flow. *Proc. 16th Intern. Symp. Shock Tubes and Shock Waves*, Aachen, Germany, July 26-31, pp. 243-249, 1987.

[14]Osiptsov A.N., Shapiro E.G., Effect of dispersed admixture on the structure of the boundary layer on a blunt body in hypersonic flow. *Izv. Akad. Nauk SSSR, Mekh. Zhidk. Gaza*, No. 5, pp. 55-62, 1986.

[15]Osiptsov A.N., Mathematical modeling of dusty-gas boundary layers. *Appl. Mech. Rev.,* v. 50, No. 6, pp. 357-370, 1997

[16]Vasilevskiy E.B., Yakovleva L.V. The tangential gas injection as the means of heat protection of a blunt body streamlined by dusted gas. *Proceeding of 3rd International conference for Aero Space Sciences (EUCASS)* , July 6-9 2009, Versailles, France.

[17] Vasilevskii E.B., A.V. Chirikhin, Osiptsov A.N. Heat transfer to a stagnation region of a blunt body in a hypersonic flow with an admixture of solid particles. // *Proc. 3d Europ. Symp. Aerothermodyn. Space Vehicles. ESTEC*, Noordwijk, The Netherlands, 24-26 November 1998. ESA SP-426, p. 301-307.

[18]Fay J. A., Riddell F. R. Theory of stagnation point heat transfer in dissociated air. *J. Aeronaut. Sci.,* 1958, No 2, P. 73-85.

Copyright Statement